Astron. Astrophys. 355, 1103–1114 (2000)

ASTRONOMY AND ASTROPHYSICS

Optical long-slit spectroscopy and imaging of OH 231.8+4.2

C. Sánchez Contreras[1,3], **V. Bujarrabal**[1], **L.F. Miranda**[2], **and M.J. Fernández-Figueroa**[3]

[1] Observatorio Astronómico Nacional (IGN), Ap. 1143, 28800 Alcalá de Henares, Spain ([sanchez, bujarrabal]@oan.es)
[2] Instituto de Astrofísica de Andalucía, CSIC, Ap. 3004, C/ Sancho Panza s/n, 18080 Granada, Spain (lfm@iaa.es)
[3] Departamento de Astrofísica, Facultad CC. Físicas, Universidad Complutense, 28040 Madrid, Spain ([sanchez, mjf]@astrax.fis.ucm.es)

Received 4 June 1999 / Accepted 28 December 1999

Abstract. We present optical long-slit spectra and complementary broad and narrow band images of the bipolar protoplanetary nebula OH 231.8+4.2. Absolute J2000 coordinates have been calculated for our maps from the position of nearby stars. Our maps of the optical continuum show the spatial distribution of the starlight scattered by dust grains. This component is found to be highly elongated along the nebular axis, with a structure very similar to that of the molecular emission. Flux variations with time of the red continuum emission are detected. Our long-slit spectroscopy of Hα and other atomic lines reveals wide spectral profiles and, in general, a complex spatial and spectral emission distribution. The emission arises from two broad lobes and is shifted toward shorter (north lobe) and longer wavelengths (south lobe), indicating that the gas is flowing outwards at high velocity. The clumpiness of the emission nebula is remarkable. A simple model has been used to describe the complex structure and kinematics of this source. Our model suggests that, in addition to the two extended, hollow lobes identified in the Hα images, a smaller, bubble-like expanding structure should lie inside the south lobe. A comparison of the emission line spectrum with predictions of theoretical shock models confirms that the optical lines have been shock excited. We have estimated the electron density of the lobes and deduced the total ionized mass of the nebula, obtaining a low value of $\sim 5\times10^{-4}\ M_{\odot}$. We interpret the shaping and evolution of OH 231.8+4.2 in the wind interaction scenario for planetary nebulae formation. The peculiar structure and kinematics of the molecular outflow and the ionized envelope are explained in terms of a shock regime transition: the well collimated molecular outflow and the different components of the optical nebula would consist of circumstellar material swept-up by a unique shock in a radiative, and non-radiative regime, respectively. Finally, we briefly discuss the controversial evolutionary status of OH 231.8+4.2.

Key words: stars: AGB and post-AGB – stars: individual: OH 231.8+4.2 – stars: mass-loss – stars: circumstellar matter – stars: late-type

Send offprint requests to: C. Sánchez Contreras

1. Introduction

As far as we know, OH 231.8+4.2 consists of (at least) one evolved star surrounded by a remarkable bipolar nebula. This object has been extensively studied with different observational techniques. The optical nebula is formed by a pure-line emission component in addition to a reflection nebulosity. The emission nebula is composed of two extended lobes, roughly oriented in the north-south direction, which are expanding from the center of the nebula (Reipurth 1987). The spectrum of these lobes is found to be very similar to those of Herbig-Haro (HH) objects, i.e. with strong atomic forbidden lines of low excitation (Cohen et al. 1985). Such emission spectra are indicative of excitation by shock waves.

Spectrophotometry of the reflection nebula leads to the spectral classification of the central star as M 9 III (Cohen 1981). Recently, a direct image of such a star has been obtained by Kastner et al. (1998). These authors find that it appears as a typical Mira variable with a pulsation period of about 700 days.

The neutral envelope of OH 231.8+4.2 has also been studied through the emission of different molecules (Morris et al. 1987; Jackson & Nguyen-Q-Rieu 1988; Alcolea et al. 1996; Sánchez Contreras et al. 1997). This envelope is found to be very cold and massive ($\sim 1 M_{\odot}$) and affected by a strong axial expansion similar to that found in the optical line emission nebula. It is remarkable that, in contrast to the atomic material, the molecular gas is highly restricted to the symmetry axis of the nebula (Alcolea et al., in preparation, hereafter paper III).

The inclination of the OH 231.8+4.2 symmetry axis with respect to the plane of the sky is estimated to be $\sim 36°$, with the North lobe pointing toward the observer. The distance to the source is about 1500 pc, and its total luminosity is $\sim 10^4\ L_{\odot}$. These values are relatively well known for this source; the methods used to their determination are described in detail in Reipurth (1987), Bowers & Morris (1984), Kastner et al. (1992), Shure et al. (1995), and references therein.

It is generally accepted that most of the nebular material of OH 231.8+4.2 was ejected by the central star during its evolution through the asymptotic giant branch (AGB). In this evolutionary stage the star generates a circumstellar envelope that expands isotropically at low velocity. The present bipolar morphology and kinematics of OH 231.8+4.2 are thought to be the result

of the interaction between recent, fast and bipolar jets, and the previous AGB envelope (Reipurth 1987; Sánchez Contreras et al. 1997). This interaction leads to the axial acceleration of the AGB circumstellar envelope that so develops a conspicuous axial symmetry. The bipolarity and the high velocities reached by the gas are both widespread characteristics of protoplanetary and planetary nebulae. Hence, from the properties of its nebula, OH 231.8+4.2 seems to have left behind the AGB, being at present somewhere in the evolutionary path toward the Planetary Nebula (PN) phase. On the other hand, the late spectral type of the central star of OH 231.8+4.2 suggests that it is still on the AGB. Therefore, the contradiction between the apparent status of the star (AGB) and the nebula (post-AGB) prevents a simple description of the evolution of this object (see a brief discussion in Sect. 6).

In order to get insights into the nature and formation of OH 231.8+4.2 we have obtained optical long-slit spectra and direct broad and narrow band images. These data, in combination with molecular observations, allow us to analyze in detail the structure, kinematics, and physical conditions of the nebula. Finally, these results are discussed in terms of the evolution and shaping of the nebula.

2. Observations and data reduction

2.1. Optical imaging

We have performed narrow and broad band imaging of OH 231.8+4.2. Two sets of observations were done in different epochs: on November, 27th and 28th, 1997, and on December, 11th, 1998. The first set of observations was done with the 1 m Jacobus Kapteyn Telescope (JKT) of the Roque de los Muchachos Observatory (La Palma, Spain). The detector was a TEK CCD with 1124×1124 24 μm squared pixels. The scale on the focal plane was $0\farcs33$/pixel. Three filters were used: Hα ($\lambda_0 \simeq 6553$ Å, FWHM $\simeq 62$ Å), Harris R3 ($\lambda_0 \simeq 6400$ Å, FWHM $\simeq 1500$ Å) and Harris B3 ($\lambda_0 \simeq 4300$ Å, FWHM $\simeq 1100$ Å). The Hα filter also includes emission from the [N II] doublet (6548, 6583 Å). The transmission of the filter is the same for the [N II] 6548 Å and Hα lines, $\simeq 60\%$, and is of about 38% for the [N II] 6583 Å line. The integration times were 1800 s, 3600 s and 1500 s for the Hα, R and B images, respectively. The weather was good during the observations, and the seeing was of about $1\farcs3$ except for the Hα image ($\simeq 2''$). In December 1998, a narrow band Hα image was obtained using the Wide Field Camera (WFC) of the 2.5 m Isaac Newton Telescope (INT) of the Roque de los Muchachos Observatory. The detector was an EEV CCD of 2048×4100 pixels, each pixel of 13.5×13.5 μm^2, giving a scale at the prime focus of $0\farcs333$/pixel. The central wavelength and width of the Hα filter are $\lambda_0 \simeq 6568$ Å and FWHM $\simeq 95$ Å, respectively, so the images include Hα and [N II] doublet emission. The filter transmission for these lines is $\sim 85\%$. The exposure time was 3600 s. Weather conditions were good and the seeing was $\sim 2\farcs2$.

All the images have been bias and flat-field corrected with standard techniques using IRAF [1]. The Hα images have been flux calibrated by comparison with our calibrated long-slit data (Sect. 2.2). In these images the continuum emission has not been subtracted, such a contribution being higher in the INT image due to the large width of the filter. Broad band images, R and B, could not be flux calibrated, and only relative fluxes are given. Astrometry of our images has been done using the coordinates of the field stars given by the HST Guide Star Catalogue (GSC) produced by the Space Telescope Science Institute. The errors on the given absolute positions are expected to be smaller than $1''$. We present the results of these observations in Fig. 1. In this figure we show smoothed JKT Hα and B images, the effective spatial resolution achieved being $\simeq 2\farcs6$ and $2''$, respectively.

2.2. Optical long-slit spectroscopy

Long-slit spectra of OH 231.8+4.2 were obtained on January, 17th and 18th, 1998, using the IDS spectrograph of the 2.5 m INT of the Roque de los Muchachos Observatory. The detector was a TEK 24 μm CCD with 1124×1124 pixels. The 500 mm camera and gratings R1200Y and R1200B were employed for the spectra in the red and blue regions, respectively, providing a dispersion of $\simeq 17$ Å mm^{-1}. Six slit positions were observed at position angles (PAs) 21° (the symmetry axis of the object), 25°, 31°, 56°, 111° and 162°. These slit positions are shown in Fig. 1 overimposed on the JKT Hα image of OH 231.8+4.2. Note the presence of field stars entering several slits. At PA 21° we observed the [N II] 6548,6583, Hα and [S II] 6716,6731 lines with an exposure time of 7100 s, the [O I] 6300,6363 lines with 2700 s, the [O II] 3726,3729 lines with 3600 s, and the Hβ and [O III] 4959,5007 lines with 2700 s. At the other PAs, the [N II] 6548,6583, Hα and [S II] 6716,6731 lines were observed with exposure times ranging from 1800 s to 5200 s. The slit was $1''$ (0.18 mm) wide and long enough to cover the whole nebula. The data were reduced using standard procedures for long-slit spectroscopy within the IRAF package, including bias subtraction, flat-fielding correction and sky subtraction. Removal of cosmic rays and bad pixels was done using the REDUCEME [2] spectroscopic reduction package (Cardiel & Gorgas, in preparation). We have used CuNe and CuAr lamps for wavelength calibration. The achieved spectral resolution (FWHM) ranges approximately between 38 ± 2.5 km s^{-1}, at Hα, and 80 ± 2.5 km s^{-1}, at [O II]. Flux calibration was done using sensitivity functions derived from two spectrophotometric standard stars, HR 1544 and HR 3454, and taking into account the atmospheric extinction curve. The effective spatial resolution obtained was $\simeq 2''$.

The obtained spectra have been smoothed with a flat-topped rectangular kernel of dimensions 3×3 pixels. The smoothed spectra for the different slit positions are presented in Sect. 3.3.

[1] IRAF is distributed by the National Optical Astronomy Observatories, which are operated by the Association of the Universities for Research in Astronomy, Inc., under cooperative agreement with the National Science Foundation

[2] http://www.ucm.es/info/Astrof/reduceme/reduceme.html

The effective spectral resolution of the resulting spectra is poorer than the nominal one by a factor ~ 1.3. However, the resolution in the spatial direction has not been degraded, since the size of the smoothing window in this direction was smaller than the local seeing.

3. Observational results

3.1. Optical imaging

In Fig. 1 we show the Hα images obtained with the INT and JKT, and R and B images of OH 231.8+4.2. We recall that in the Hα images the continuum has not been subtracted (Sect. 2.1). The asterisk in Fig. 1 corresponds to the maximum of the SO_2 emission (Jackson & Nguyen-Q-Rieu 1988) which coincides, within $1''$, with the CO, SiO maser and the millimeter continuum emission maxima (Alcolea et al. 1996; Sánchez Contreras et al. 2000) and, approximately, with the position of the Mira star inside OH 231.8+4.2 (Kastner et al. 1998). The coordinates of this point are (J2000): $07^{\rm h}42^{\rm m}16\overset{\rm s}{.}9$, $-14^\circ 42' 49''$.

Our two Hα images confirm the known general structure of OH 231.8+4.2 (Sect. 1), also providing more details on it. The nebula consists of two extended lobes emerging from an obscured region inside of which the central star lies. The lobes are aligned and oriented in the sky $\sim 21^\circ$ from north to east, defining thus the symmetry axis of the nebula in this direction. The central, obscured region is thought to be a high density ring/disk lying in a plane almost perpendicular to the symmetry axis. Note the north-south asymmetry of the nebula, the south lobe being more than 2 times larger than the northern one. The complexity is also greater in the southern lobe. The relatively intense, bow-shaped structure, at the end of this lobe is particularly remarkable. Note also the clump lying slightly beyond this structure.

The R and B images in Fig. 1 correspond to the continuum emission centered at 6400 and 4300 Å, respectively. The emission in the R image arises from two inner, relatively narrow nebulosities located at both sides of the central star and aligned with the nebular axis, the southern being intrinsically brighter than the northern one. The size of the south nebulosity in R is about $\simeq 4''\times 4''$ at half maximum. Note that in the continuum R image there is no counterpart of the outer, extended lobes seen in the Hα image, a fact which clearly establishes their pure-line emission nature. The emission distribution is similar in the B image. However, in this case, the southern nebulosity is visible up to distances of $\sim 38''$ from the central star, indicating that the emission from regions near the equator in the south lobe is redder than that arising from distant regions. The brightness contrast between the north and south inner nebulosities is also higher in the R image than in the B image. We think that the previous color differences are due to an extinction effect: the blue photons arising from the brighter, inner south nebulosity are selectively absorbed by the equatorial condensation of material which seems to be present at the nebula center (note that the north lobe is inclined toward the observer).

The described distribution of the continuum emission, in two narrow nebulosities, has been found to be very similar to that of the CO emission (paper III). Since the optical continuum is the light of the central star reflected by dust grains, as demonstrated by Cohen (1981), Cohen et al. (1985), and our spectroscopic observations (see Fig. 2 and below), such a coincidence indicates that molecular gas and solid particles follow almost the same distribution along the nebula axis.

In the Hα images we also find emission from the two inner nebulosities seen in the continuum images. The line emission in these regions is very weak, as our long-slit spectra demonstrate (see below), therefore, the intensity detected with the Hα filters in these two condensations is dominated by the stellar continuum reflected by the nebula. Since the source illuminating the nebula is a Mira variable star (Sect. 1), the brightness of these nebulosities is expected to change with time. In fact, as we can see in Fig. 1, these nebulosities are brighter in November, 1997 (JKT image) than in December, 1998 (INT image). These intensity differences cannot be explained in terms of the different filter width and seeing between the two images since, in that case, a higher continuum intensity would be expected for the INT image, which was obtained with a larger filter width and smaller seeing than the JKT image. Kastner et al. (1992) estimate a pulsation period for the Mira of 700 days from the variability of the stellar NIR emission reflected by the nebula. Accordingly, the JKT and INT observations would be separated approximately by 0.5 stellar periods. The relatively strong intensity contrast of the continuum found between our two observations, which is approximately a factor 4 (~ 1.5 mag) at the ($0''$, $0''$) position, suggests that the JKT observations were done close in time to the intensity maximum. In fact, based on the light curve presented in Kastner et al., a NIR maximum should have occurred in November, 1997, supporting the previous idea.

3.2. The spectrum of the reflection nebulosity of OH 231.8+4.2

From our long-slit data we have extracted the continuum spectrum of OH 231.8+4.2. Such a continuum emission is only detected at red wavelengths, from ~ 6060 to 6770 Å, and reaches its maximum intensity in the southern nebulosity seen in the R image – around the ($0''$, $0''$) position in Fig. 1. The spectrum of a $1''\times 1''$ region centered at offset ($0''$, $0''$), in the range 6370–6770Å is shown in Fig. 2. This spectrum is the average of those obtained from the six slit positions and, as already mentioned, corresponds to the scattered light of the central star obscured by the inner regions of the nebula. Several molecular bands (TiO, CaH, and VO) can be identified in the continuum spectrum (Fig. 2); the comparison with standards confirms the M 9 III spectral type of the star (Cohen 1981).

The continuum spectrum of OH 231.8+4.2 in the 6060–6460 Å range is consistent with the spectral classification of the star but does not provide any additional information. The average flux in this wavelength range at the ($0''$, $0''$) position is $\sim 8.6\times 10^{-18}$ erg s^{-1} cm^{-2} Å^{-1} arcsec^{-2}. For the continuum level in the ranges 3470–3890 Å and 4760–5170 Å at the same position, we can only give upper limits, 8.5×10^{-18} and 6×10^{-18} erg s^{-1} cm^{-2} Å^{-1} arcsec^{-2}, respectively. For the fainter north reflection nebulosity seen in our optical images

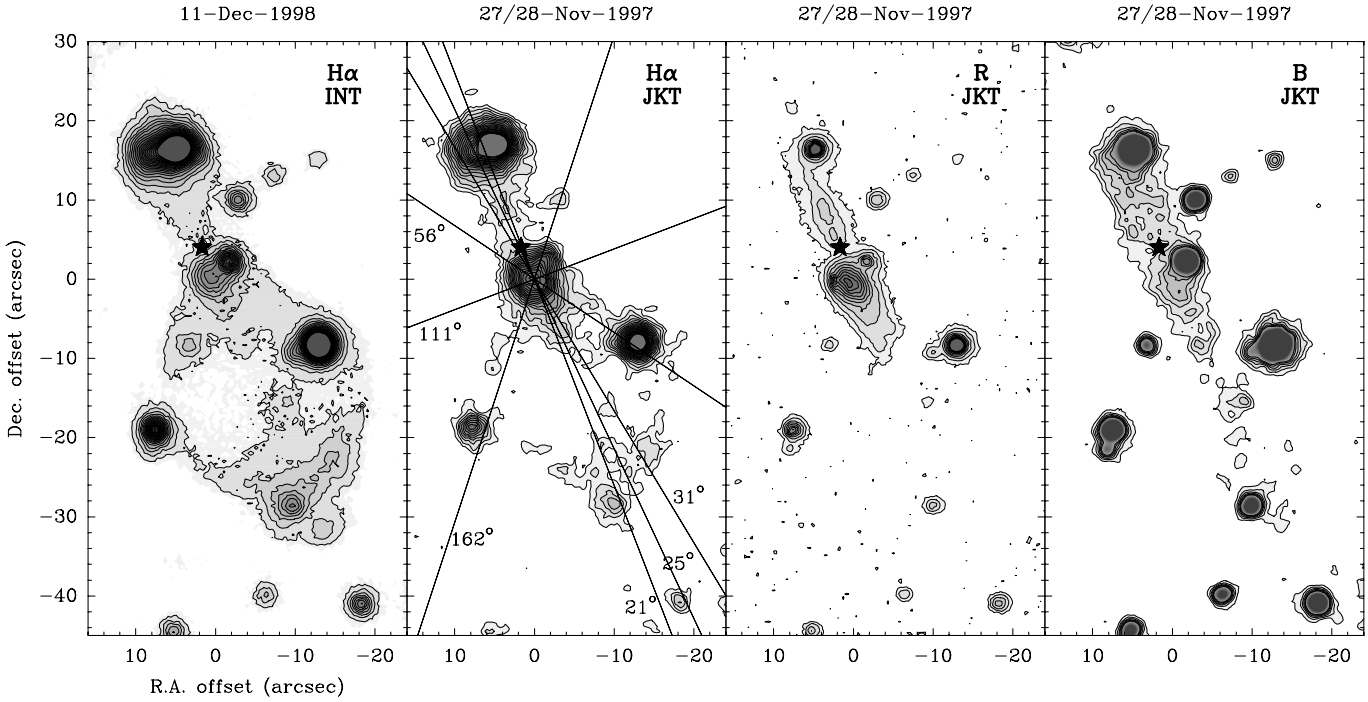

Fig. 1. Hα+[N II], R and B images of OH 231.8+4.2. For the INT (JKT) Hα image, contours are 10^{-16} (2×10^{-16}) to 2×10^{-15} by 10^{-16} erg s^{-1} cm^{-2} arcsec^{-2}. For the broad band images, contour levels relative to the flux at (0″, 0″) in each case are: 10% to 100% by 10% for R, and 30% to 130% by 20% for B. The coordinates of the asterisk position, which represents the central star location, are (J2000): $07^{\rm h}42^{\rm m}16\overset{\rm s}{.}9$, –14°42′49″. The coordinates of (0″, 0″), the point where the optical continuum maximum of OH 231.8+4.2 occurs, are (J2000): $07^{\rm h}42^{\rm m}16\overset{\rm s}{.}8$, –14°42′53″. The 6 different slit positions used for spectroscopy are shown on the JKT Hα image.

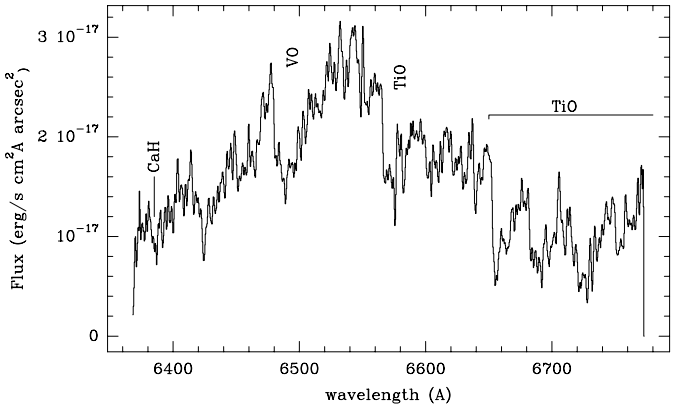

Fig. 2. Spectrum of the stellar light reflected by the nebula at the (0″, 0″) position (Fig. 1) in January, 1998.

– around the (4″, 8″) position in Fig. 1 – the flux is found to be 1.9×10^{-18} erg s^{-1} cm^{-2} Å^{-1} arcsec^{-2} averaged between 6370 and 6770 Å. We recall that these values correspond to January, 1998. At this epoch the optical continuum was ~ 1.3 times weaker than in November, 1997, when the NIR and optical continuum maximum presumably occurred (Sect. 3.1).

3.3. Long-slit spectroscopy

In Fig. 3 the Hα and [N II]6583 long-slit spectra obtained for the six different slit orientations are shown in a position vs. velocity representation. As we see in Fig. 1, the slit at PA 21°, coincides with the symmetry axis of the nebula. Slits at PAs 25° and 31° are also near this axis, while those at PAs 56° and 162° are located on the edges of the extended south lobe. We also placed one slit in the direction perpendicular to the symmetry axis of the source, PA 111°. We have detected continuum and line emission for all the slit positions except for PA 111°, where only the continuum of OH 231.8+4.2 (scattered starlight, Sect. 3.2) is present. Note the presence of the continua of field stars at $\sim -30''$ at PA 21° (see discussion in Sect. 5.1), at $\sim -20''$ and $\sim$+10″ at PA 162°, and at $\sim -15''$ at PA 56° (see Figs. 3, 4 and 1). We have defined the origin of the spatial scale of our long-slit spectra at the point where the OH 231.8+4.2 continuum reaches the maximum intensity, coincident with the (0″, 0″) position in our optical images (Fig. 1). So, the central star (see Fig. 1) should be approximately located at +4″ on the PA=21° direction. As we see in Fig. 3, no stellar continuum emission is present at this position, indicating a high light extinction in this direction probably due to the presence of a dense, equatorial belt of dust.

We have found line-emission features with broad profiles and, in general, very complex structure. In the spectra obtained with the slit placed approximately on the symmetry axis (PAs 21°, 25° and 31°), the line emission arises from the broad north and south lobes seen in the Hα image (Fig. 1). The emission from the north/south lobe is blue/red-shifted with respect to the systemic velocity ($V_{\rm sys}$ $\sim$ 33 km s^{-1}, in our case $V_{\rm sys}$ corresponds to the velocity of the star and of the central, very mas-

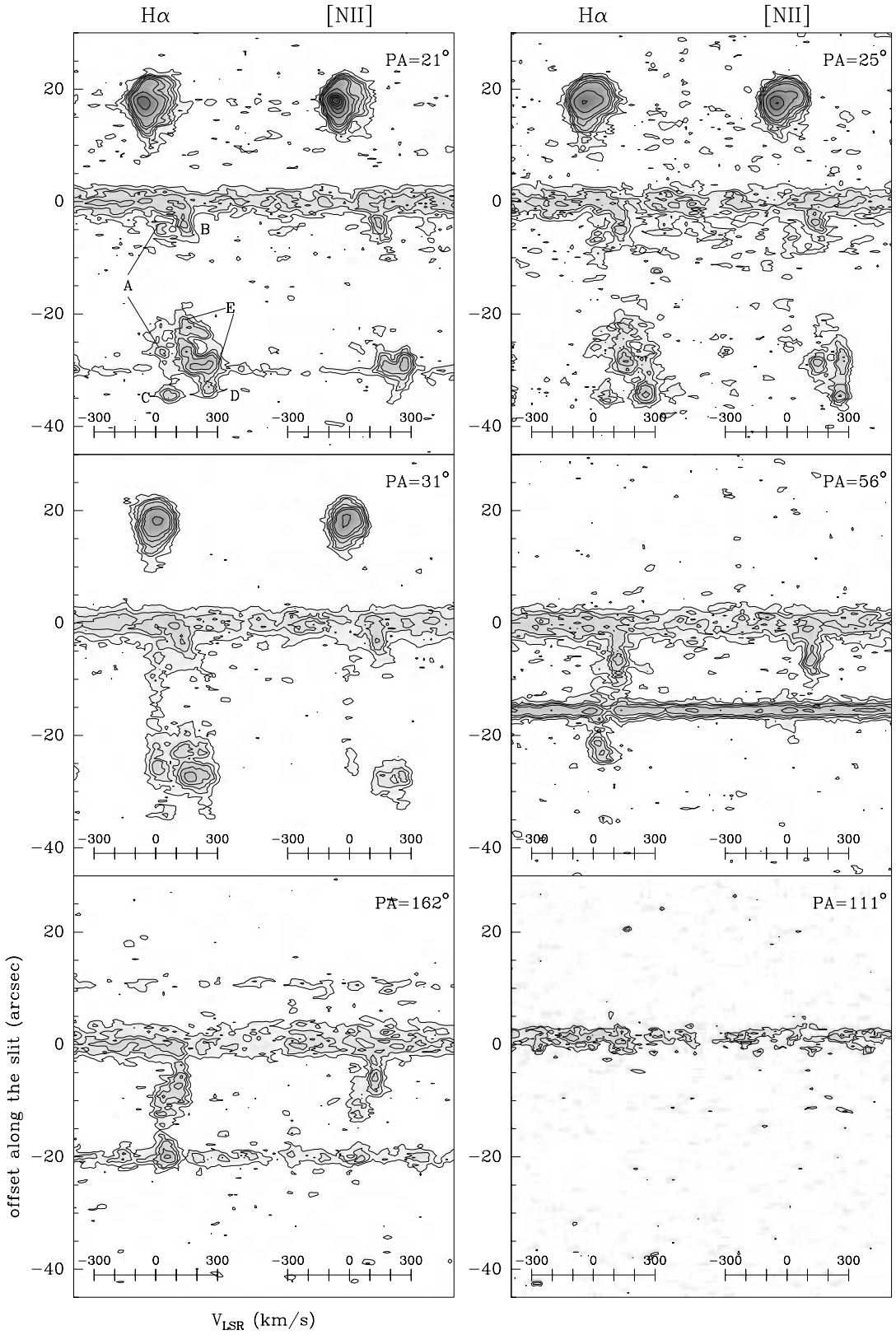

Fig. 3. Long-slit Hα and [N II]6583 spectra for the different slit orientations (PAs of the slit are indicated on the top right corners of each box). Contours levels are 0.76, 1.51, 3, 6, and 12 to 73 by 12, in units of 10^{-17} erg s^{-1} cm^{-2} Å^{-1} arcsec^{-2}. For the PA=111° spectrum, the 0.76 contour is not drawn because of the higher noise level. The velocity (LSR) scale is shown at the bottom of each emission line. The systemic velocity is $\sim$33 km s^{-1}. The main spectral features identified in the south lobe are noted A, B, C, D, and E in the PA=21° spectrum. Note the scattered stellar continuum at 0″ position.

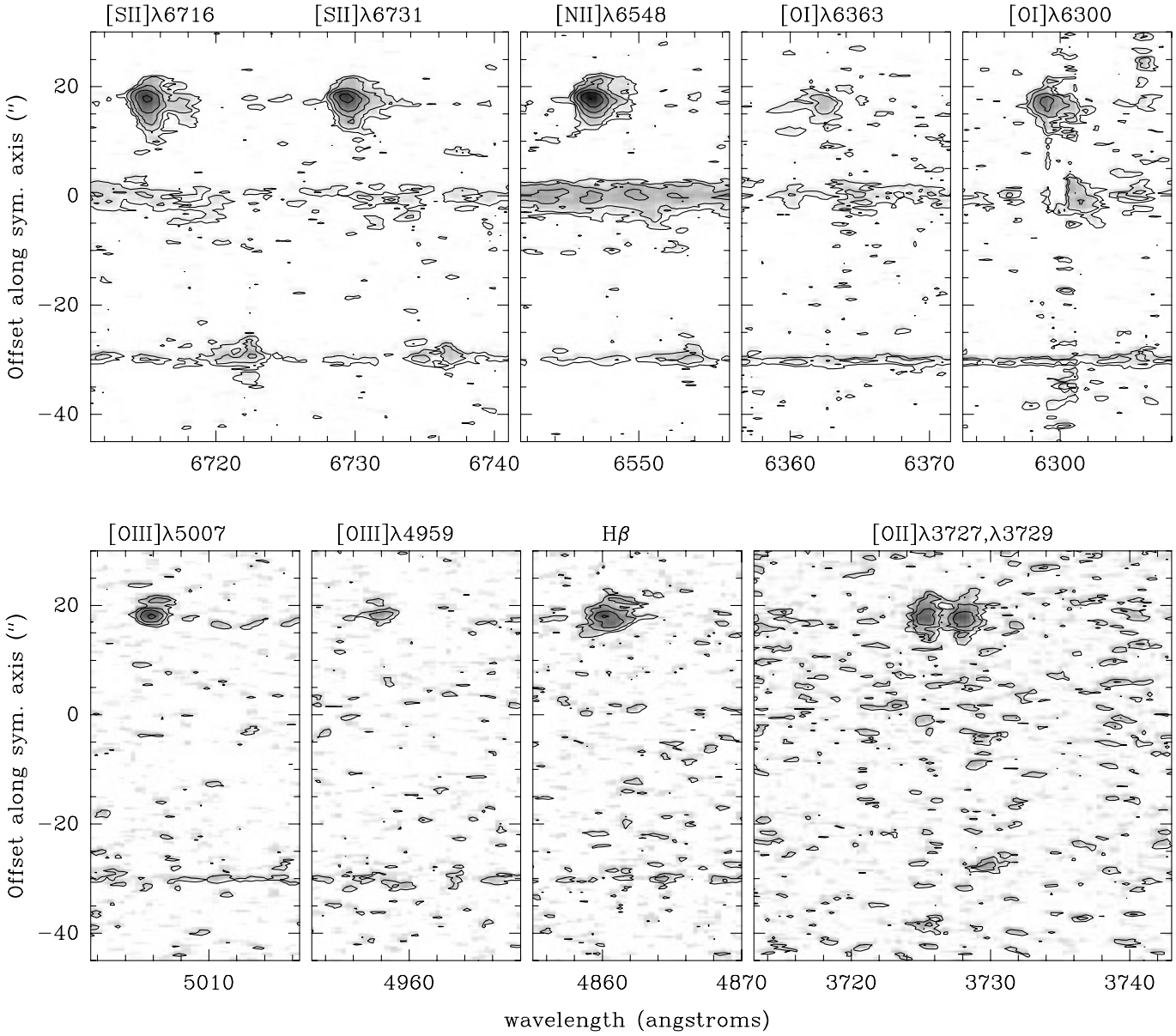

Fig. 4. Long-slit spectra of the different nebular lines (except for Hα and [N II]6583, shown in Fig. 3) detected along the symmetry axis of the nebula (PA=21°). Contours are the same as in Fig. 3, except for the bottom spectra where the first contour is not drawn because of the noise. Note the residual atmospheric contamination in the 6300Å line.

sive CO clump, see e.g. Sánchez Contreras et al. 2000; Morris et al. 1987; Alcolea et al. 1996), the lines showing a total LSR velocity range of ~ 500 km s^{-1}. This large line width indicates that the gas is flowing outwards at high velocity along the lobes of OH 231.8+4.2. The distribution of the emission arising from the extended south lobe is particularly complex. Here we identify different spectral features, labeled A, B, C, D, and E on the PA 21° Hα spectrum (Fig. 3 and Fig. 5, right panel). These features are also present with similar shapes in the PA 25° and PA 31° Hα spectra (Fig. 3). Note that in the PA 31° spectrum the emission feature A, around the systemic velocity, approximately extents from 0″ up to -30″, while in the PAs 21° and 25° spectra no emission has been detected between ~ -8″ and ~ -20″. This is in agreement with the Hα image, in which the west side of the south lobe appears globally more intense than the east one. The line spectrum obtained with the slit placed at PAs 162° and 56°, is formed by two spatially extended components displaced in velocity, with no significant velocity changes along each component. Due to the position of the slits over the nebula, the emission in these spectra arises entirely from the south lobe.

In Fig. 4 the spectra of the different emission lines detected for the PA 21° slit orientation are presented, except for the already discussed Hα and [N II]6583 lines. In the north lobe, the emission of the different lines is extended, and presents a spatial and spectral distribution similar to that of the Hα line. From the

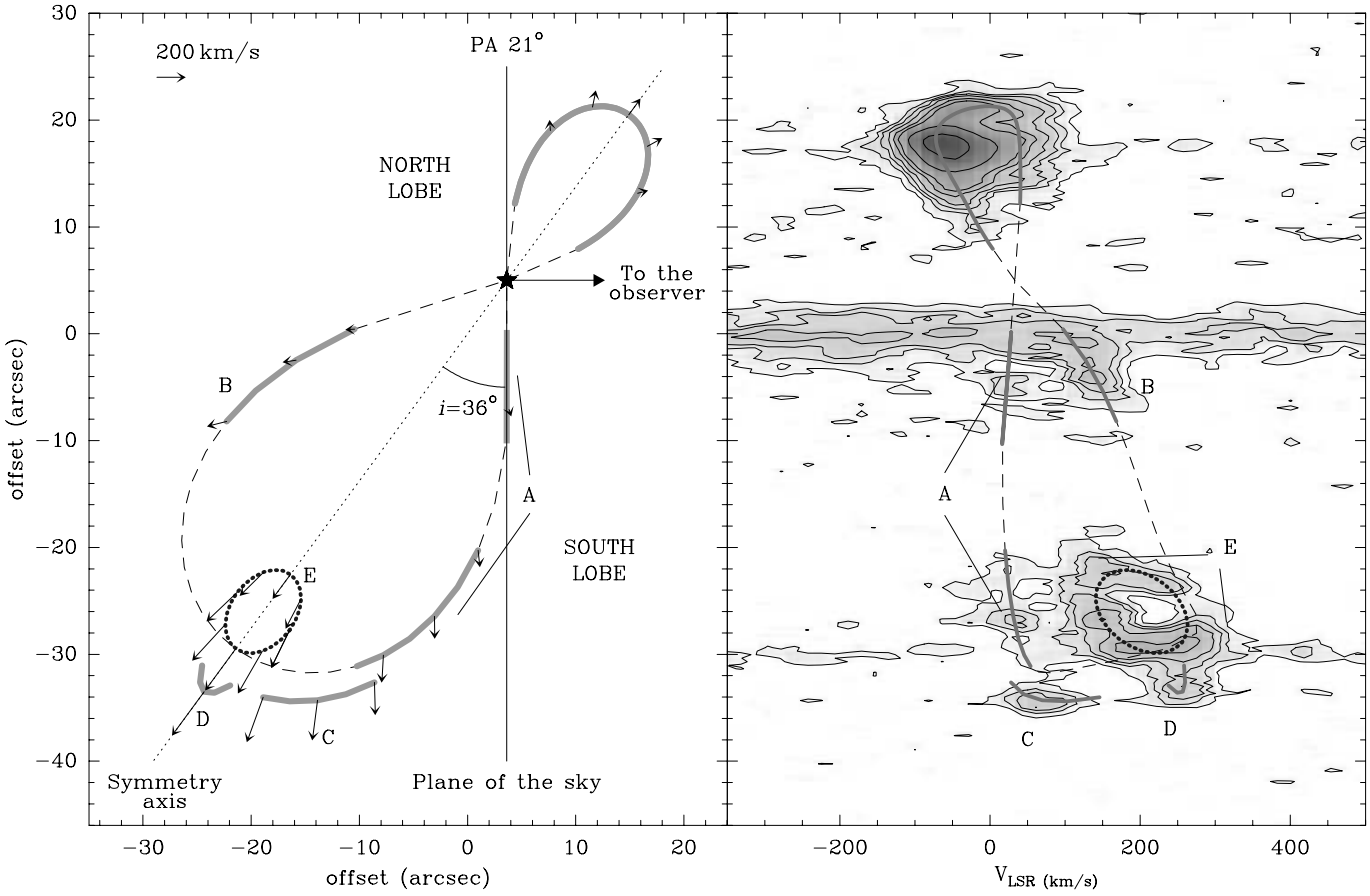

Fig. 5. Left panel: schematic geometry of OH 231.8+4.2 deduced from the model fitting. In this diagram, 1″ corresponds to 2.2×10^{16} cm (see text). The extended lobes (*solid* and *dashed lines*) and the bubble-like expanding structure (*dotted lines*) which form the nebula are indicated. This plot represents a cut of the nebula by a plane perpendicular to the plane of the sky in the direction of PA 21°. The velocity field is indicated by small arrows. Right panel: Hα spectrum for the PA=21° slit orientation (contours and labels are the same as in Fig. 3) and position-velocity diagrams resulting from the model fitting.

south lobe only emission from Hα, the [N II] and [S II] doublets, and the [O I]6300 line (close to the equator) have been detected. In these cases, the emission is also spatially extended and shows velocity shifts that are similar for all the detected lines. Note the presence of residues of the atmospheric emission subtraction in the [O I] spectrum (clearly seen at 6300 and 6306 Å). Due to these remnants, the origin of the 6306 Å emission detected at offset $\sim -30''$ cannot be determined. Considering its spatial position and velocity, it could be emission from the south lobe, however, it could also be a sky line subtraction artifact. The red stellar continuum reflected by the nebular dust (Sect. 3.2) can be seen between 6060 and 6770Å in Fig. 4 at offset 0″.

4. Structure and kinematics of OH 231.8+4.2

In order to understand the structure and kinematics of the atomic envelope of OH 231.8+4.2, we have constructed a simple kinematical model which reproduces the different Hα features identified in our long-slit spectra. Although the model has been mainly applied to the PA 21° spectrum, we have checked that it also qualitatively explains the Hα spectra at the other slit orientations. Our model calculates the position-velocity (p-v) diagram assuming a certain morphology for the envelope (compatible with our direct images) and a velocity field, and also taking into account the inclination of the nebula to the plane of the sky ($i \sim 36°$, Sect. 1). The dynamical origin of such a morphology and its kinematics will be discussed in Sect. 6.

We have found that the nebula should be made up of, at least, two superimposed structures, in order to reproduce the complex Hα features. In Fig. 5, left panel, we show a sketch of the different components required in our model, to which we will refer as extended lobes (*solid line*) and bubble-like expanding south structure (*dotted line*). The extended lobes are clumpy (see below), the regions from which we do not observe line emission being also indicated in this figure by dashed lines.

We are assuming in our model that the extended lobes are hollow and show an overall axial symmetry, as suggested by the optical appearance of OH 231.8+4.2. The Hα image also indicates that these lobes are approximately conical near the equator and rounded at each end. The cone opening angles, determined from the Hα image after deprojection, are $\sim 33°$ and $\sim 39°$ for the north and south lobes respectively. The total (deprojected) length of the lobes has been estimated from the fit of

the synthetic p-v diagrams to the spectra. (We will use in this section arcseconds as units of the spatial length to better compare with observations; at a distance of 1500 pc, $1''$ is equivalent to 2.2×10^{16} cm.) In the case of the north lobe the fit leads to a single value of the axial extent, $\sim 20''$ (4.4×10^{17} cm), which is also compatible with the optical images of the nebula. For the south lobe, different axial sizes can reproduce (with the adequate velocity field) the long-slit spectra, however, we have ruled out those which do not match the Hα image (assuming axial symmetry). Thus, the total axial extent of the south lobe is found to be about $50''$ (1.1×10^{18} cm), including some mass condensations detached from the lobe that lead to features C and D (see Fig. 5 and below). The observed patchy emission (that is obvious both in the Hα image and spectra) suggests that there are strong density and/or excitation contrasts from one region to another. In fact, we have found that the intensity distribution of the lines in the south lobe cannot be explained by projection effects with a uniform density distribution. Therefore, we have assumed a clumpy structure for the OH 231.8+4.2 envelope, that could be even broken in several clumps (see *solid* and *dashed lines* in Fig. 5).

The main velocity component of our kinematical model for the extended, clumpy lobes is a radial expansion with the modulus of the velocity at each point being proportional to the distance to the central star. Actually, in our long-slit spectra we can see that the outer regions of the nebula flow at higher velocity than the inner ones, following a velocity gradient which is almost constant. Moreover, a similar velocity field is present in the molecular envelope of OH 231.8+4.2 (Sánchez Contreras et al. 1997). We have found that the velocity shift between features B and A strongly restricts the velocity gradient to values between $\sim$ 4.5 and 5.5 km s^{-1} arcsec^{-1} (deprojected) for the assumed source geometry. Then, in our model, we have assumed a velocity gradient of $\sim$5 km s^{-1} arcsec^{-1} which is also adequate to globally explain the velocity shift between the emission from the north and south lobes. However, such a velocity field cannot reproduce the large total width of the Hα line arising from each lobe ($\sim$ 300 km s^{-1}). The velocity field that best reproduces the general Hα profile is found to be the composition of the previous radial velocity field and a spherical expansion originated inside of the extended lobes. An expansion velocity law of the type $V_{exp} \propto r^{-1}$, where r is the distance to the expansion center, yields the best fitting of the line spectra. For the south lobe the expansion center coincides with the center of the bubble-like expanding structure (see Fig. 5). For the north lobe the expansion center is located on the symmetry axis at $\sim 16''$ from the central star. The resulting velocity field adopted in our model is indicated by small arrows in Fig. 5 (left panel). The predicted p-v diagram is also shown in the right panel of the same figure.

In the Hα spectra along the symmetry axis, there are two relatively isolated, compact features approximately located at an offset $\sim -35''$ and LRS velocities 70 and 260 km s^{-1}. These features, noted C and D respectively, are also present in the PAs 25° and 31° long-slit spectra, indicating that the regions responsible for these emission features are somewhat extended in the direction perpendicular to the axis. In fact, these features are spatially coincident with the southernmost emission region, $\sim 6''$ wide, seen in the Hα image (Fig. 1). The morphology and kinematics that we propose to explain these features are indicated in Fig. 5; both features would be originated by clumps of gas detached from the south lobe which flow following the general velocity field of this lobe. We have illustrated the clump responsible for the D feature by a small, curved structure according to the appearance of this region in the Hα image (remember that we are assuming axial symmetry). The predicted p-v diagram is shown in Fig. 5.

The bubble-like expanding structure lying inside the south lobe (Fig. 5, *dotted line*), is introduced in our model to explain the remarkable feature E found in our Hα spectra (PAs 21°, 25° and 31°). This feature, characterized by a relative minimum at $\sim -26''$, $\sim$ 220 km s^{-1}, arises from the bright, bow-shaped southern structure seen in the Hα image. In our model, the velocity field for the shell is the composition of a radial velocity field (as for the extended lobes) and a bubble-like expansion. However, in this case the (deprojected) velocity gradient must lie in the interval $\sim$ 7 and 8 km s^{-1} arcsec^{-1} ($>\sim$ 5 km s^{-1} arcsec^{-1}, found for the extended lobes) to properly reproduce feature E. The expansion velocity of this structure is about 35 km s^{-1} (see the resulting velocity field in Fig. 5, right panel).

We would like to stress that the representation of the envelope of OH 231.8+4.2 given in Fig. 5 is merely schematic, and that we do not intend to describe in detail the morphology and kinematics of the different sub-structures of the nebula. We have represented the extended lobes by lines, the thickness of which does not necessarily correspond to the actual thickness of the walls of the lobes. In fact, if the top of the north lobe is assumed to be 3–4$''$ thick, we can better reproduce the large velocity dispersion observed at offset $\sim$ +18$''$, for the velocity field described above. This wide line profile can also be due to a large velocity dispersion as would be expected if a fast, collimated wind is impinging on this region (see Sect. 1).

On the other hand, the structures previously described are not the only ones that lead to a good fit of the Hα emission features. We have found other more or less similar morphologies for the different sub-structures in the envelope which, with the appropriate velocity field, predict features compatible with the observations. Here, we have presented the simplest structures that preserve axial symmetry, after comparison of the data for all slit positions with the Hα images.

5. Physics of the emission nebula

5.1. Excitation conditions: Importance of shocks

In Table 1 we show the observed fluxes (F_λ) of the detected nebular lines in the lobes of OH 231.8+4.2. These fluxes have been obtained from the PA 21° spectrum integrating along the slit ($1''$ wide) and over the total width of the different lines. For the north lobe the dereddened fluxes (I_λ) are also shown in the table. A logarithmic extinction coefficient c(Hβ)=0.30$\pm$0.09 has been derived for the north lobe from the observed Hα/Hβ intensity ratio, adopting an intrinsic value of 3. Note that the intrinsic relative intensity of the Hα and Hβ lines does not vary more

Table 1. Observed integrated fluxes (F_λ) for the north and south lobes of OH 231.8+4.2 obtained with the slit placed along its symmetry axis. Dereddened fluxes (I_λ) are also presented for the north lobe. Units are 10^{-15}erg s^{-1} cm^{-2} arcsec^{-1}. Flux errors are indicated between brackets.

		north lobe		south lobe
Ion	λ_0 (Å)	F_λ	I_λ	F_λ
[O II]	3727	0.64 (0.06)	1.5 (0.4)	–
[O II]	3729	0.70 (0.06)	1.7 (0.5)	–
Hβ	4861	0.97 (0.06)	2.0 (0.4)	–
[O III]	4959	0.20 (0.05)	0.4 (0.1)	–
[O III]	5007	0.55 (0.05)	1.1 (0.2)	–
[O I]	6300	0.71 (0.03)	1.2 (0.2)	$\sim$ 0.25 (0.06)[a]
[O I]	6363	0.20 (0.03)	0.33 (0.07)	$\sim$ 0.09 (0.03)[a]
[N II]	6548	1.45 (0.02)	2.3 (0.3)	0.22 (0.07)
Hα	6563	3.65 (0.02)	5.9 (0.8)	1.85 (0.07)
[N II]	6583	4.40 (0.02)	7.0 (1.0)	0.90 (0.07)
[S II]	6716	1.20 (0.02)	1.9 (0.3)	0.35 (0.07)
[S II]	6731	1.16 (0.02)	1.8 (0.3)	0.25 (0.09)

[a] Poor atmospheric line subtraction

than 10% when considering different excitation mechanisms. We have taken a wavelength dependence for the extinction from the Galactic reddening law by Howarth (1983). In the south lobe the Hβ emission is under the noise level, thus we are not able to give dereddened fluxes in this case. However, most of the south lobe fluxes come from the outer clumps, where the extinction is significantly smaller than in the north lobe (Cohen et al. 1985 and Sect. 3.1). Therefore, the dereddened values for this lobe are not expected to be very different from the measured ones given in Table 1.

As we can see, the spectrum of OH 231.8+4.2 (Figs. 3 and 4 and Table 1) is rather similar to that of HH objects, with strong forbidden lines of low excitation ions (e.g. Hartigan et al. 1987), and can be explained in terms of shock excitation. The shock nature of the emission in the lobes of OH 231.8+4.2 is mainly suggested by the high intensity of the [N II] and [S II] lines and the comparable intensities of the different oxygen lines ([O I], [O II], [O III]), which indicates a wide range of ionization states. Another argument supporting shock excitation is the fact that the central star of OH 231.8+4.2 is an M 9 type Mira. Such a cool star cannot account for the high degree of ionization observed at large distances from the center (a $\gtrsim$ 50 000 K central star would be necessary). Although there is no direct evidence, the presence of a hotter companion to the Mira has been suggested by Cohen et al. (1985), from a (weak) blue excess in the optical continuum of the nebula. However, if a hot star exists, its UV emission is not expected to be very strong, since a quite massive neutral envelope persists in the vicinity of the central star (Sánchez Contreras et al. 1997). Moreover, up to now, there are no indications of ionized material near the star (absence of free-free radio continuum or Hα emission). Therefore, we conclude that shocks are the most likely mechanism of excitation of the optical emission lines in OH 231.8+4.2.

From the obtained intensities of the different lines we have studied the characteristics of the exciting shock in the north lobe; in the weaker south lobe only a small number of lines have been detected and the upper flux limits obtained for the important Hβ and [O III] lines are not meaningful. We have plotted our data in the diagnostic diagrams by Dopita & Sutherland (1995), which can distinguish between shocks with or without a photoionized preshock region. These diagrams not only confirm the shock nature of the emission but also indicate that the emission from a photoionized precursor region is either weak or absent.

We have also compared the observed lines intensities with the predictions of the theoretical shock models by Hartigan et al. (1987). The obtained ratios for the forbidden lines of the oxygen ions are compatible with the bow-shock model 9 from Hartigan et al., within a reasonable margin of error. This model assumes preshock densities $\sim 300\,\mathrm{cm}^{-3}$ and preionization equilibrium rather than full preionization, in agreement with the results from the diagnostic diagrams by Dopita & Sutherland (1995). The relatively high intensity of the [O III] lines indicates a shock velocity of $V_\mathrm{s} \gtrsim 90$ km s^{-1}, a value which is compatible with the observed velocity of the gas in the north lobe (~ 150 km s^{-1}). The model fails, however, in predicting the intensities for the [S II] and [N II] lines, for which it yields intensities smaller by a factor ~ 3 and ~ 6, respectively, than observed. The intense [S II] and [N II] lines could be due to the enhancement of nitrogen and sulfur abundances in OH 231.8+4.2 respect to the cosmic values. This enhancement is also suggested by the large number and high abundance of N- and S-bearing molecules in this source (Morris et al. 1987; Sánchez Contreras et al. 1997). However, the lack of accuracy of the predictions could also be due to the complex shock conditions in the nebula, which cannot be accurately reproduced by the simplified bow-shock models. Finally, we note that the models by Hartigan et al. involving planar shocks cannot explain the intensities of the lines measured in OH 231.8+4.2. Moreover, planar shocks are hardly compatible with the bow-shaped emission nebula and the large velocity dispersion found in the lobes.

As previously mentioned, continuum emission near the HH-like region at offset $\sim -30''$ in the PA 21° spectrum has been found (Fig. 3). The intensity of this continuum increases toward the red wavelengths, without the least trace of the blue continuum which is expected in HH objects by two-photon and bound-free emission (Dopita et al. 1982). In the PA 21° slit orientation, offset $\sim 18''$, we also detect a fairly weak continuum. Although the signal-to-noise ratio is small in this case, we can say that it does not either increase toward blue wavelengths. We so conclude that in both cases the detected continuum is due to field stars and not to the shocked nebular gas.

The excitation conditions vary along the lobes of OH 231.8+4.2 as the analysis of the [N II]6583/Hα intensity ratio indicates. In the case of shock excitation, high values of this ratio indicate high shock velocities and, in consequence, high excitation (Hartigan et al. 1987; Dopita & Sutherland 1995). For the north lobe, we have found the highest excitation ([N II]6583/H$\alpha \sim 2$) in the region where the different lines reach their maximum intensity (at offset $\sim 18''$ and velocity

~ -60 km s^{-1} on the PA 21° spectrum, Fig. 3). In the south lobe, we have found different values of the [N II]6583/Hα ratio for the different features identified in our long-slit spectra, with features B, D, and E (Fig. 5) showing the highest values and, therefore, the highest excitation. Also, variations of the excitation conditions exist between the north and south hemispheres of the bubble-like expanding region responsible for the feature E. The interpretation of all these changes in the [N II]6583/Hα intensity ratio is not simple. For the north lobe the highest excitation is found in a relatively compact area near the symmetry axis of the nebula, probably suggesting that a collimated wind impacted there (Sects. 1 and 6). The intense [N II] emission in the south hemisphere of the bubble-like expanding structure could suggest that the regions with the highest excitation correspond to the forward shock propagating in the AGB circumstellar envelope (Sect. 6).

5.2. Electron density and ionized mass estimations

We have estimated the electron density ($n_{\rm e}$) along the symmetry axis of OH 231.8+4.2 from the red [S II] doublet intensity ratio, assuming an electron temperature of 10^4 K (note that the dependence of the theoretical intensity ratio on the temperature is weak). We have found for the north and south lobe respectively, average $n_{\rm e}$ of ~ 500 cm^{-3} and ~ 40 cm^{-3}. For the north lobe, a comparable value ($n_{\rm e} \sim 400$ cm^{-3}) has been obtained from the [O II] doublet ratio. We have found density variations inside each lobe. In particular, the region in the north lobe where the different lines reach the maximum intensity, which also coincides with the region of highest [N II]/Hα intensity ratio, is found to have $n_{\rm e} \sim 800$–900 cm^{-3}. On the other hand, in the southern lobe, the density is enhanced up to values of the order of 10^3 cm^{-3} in relatively compact regions, in contrast to regions where $n_{\rm e} \lesssim 10$ cm^{-3}. This fact confirms the clumpy density distribution in the envelope of OH 231.8+4.2.

Using the previous average values of $n_{\rm e}$, we have calculated the total ionized mass in the lobes of OH 231.8+4.2. The volume of the lobes has been estimated from the energy radiated by the Hα line, which is proportional to $n_{\rm e}^2$ and to the volume of the Hα emitting region (under well established and reasonably assumptions). The obtained volumes are compatible with the dimensions of the nebula measured from the Hα image, assuming $\sim$2–3″ thick lobes. With the previous volume values and adopting an abundance ratio He/H =0.1, the total mass of the atomic envelope of OH 231.8+4.2 has been estimated, finding a low value of $\sim 5\times10^{-4}\,M_{\odot}$. This value is about three orders of magnitude lower than the neutral gas mass ($\sim 1 M_{\odot}$, Sánchez Contreras et al. 1997). This low ionized-to-neutral gas mass ratio is much smaller than that frequently found in PNe ($\sim$1–100, e.g. Huggins et al. 1996), in which the hot central star dissociates and ionizes almost all the nebular gas.

6. Shaping and evolution of OH 231.8+4.2

The morphology and kinematics of both the neutral and the ionized components of the envelope of OH 231.8+4.2, described in Sects. 1 and 4, have been interpreted as the result of the interaction between a high velocity, bipolar wind (jet), and the circumstellar envelope of material previously ejected by the central star during the AGB phase (Reipurth 1987; Sánchez Contreras et al. 1997). This interaction gives rise to a shock wave that propagates outwards through the circumstellar medium, accelerating and heating the gas. Since the shock preferentially propagates along the direction of the jet, this interaction leads to the breaking of the spherical symmetry of the AGB envelope, which develops a remarkable axial symmetry.

Such an axial symmetry is apparent in both the molecular and the atomic envelope of OH 231.8+4.2. However, it is remarkable that the spatial distribution of these two components is completely different: the molecular gas is confined to the nebula axis while the bulk of the ionized gas is distributed in two extended, bubble-like lobes. Such a distribution of the molecular gas, on the inside of the ionized, hollow lobes, has no precedent among PPNe or PNe. In fact, in these objects the neutral material is either concentrated in an equatorial disk/torus around the central star or in an envelope that is, at least, as extended as the optical nebula (e.g. Zweigle et al. 1997; Graham et al. 1993; Bujarrabal et al. 1998a). The large extent of the shock-excited emission nebula of OH 231.8+4.2 (Sect. 5) is also unparalleled. Note, that the shock-excited emitting regions detected in the few well studied PPNe are often a set of very compact clumps located along the nebula axis (e.g. Bujarrabal et al. 1998b; Borkowski et al. 1997).

The particular distribution of the neutral and ionized material in OH 231.8+4.2 can be explained in terms of a shock regime transition from radiative into adiabatic (non-radiative). It is known that the shock regime strongly determines the morphology and the dynamical evolution of the shocked gas (e.g. Frank 1997 and references therein). In the isothermal limit (radiative shock), the thermal energy communicated to the gas by the shock wave is efficiently radiated away in a timescale shorter than the dynamical timescale of the flow. Then, the shocked material, due to the negligible thermal pressure, collapses in a dense, relatively thin shell located very close to the shock. On the other hand, when the radiative cooling is relatively not important (adiabatic shock) the thermal energy excess causes a thermal pressure increase in the shocked gas, that so expands yielding inflated shells.

We propose that the shaping and evolution of the present molecular and atomic components of OH 231.8+4.2 occurred as follows. First, the jet-like ejections impacted on a AGB circumstellar envelope dense enough to allow a quickly radiative cooling of the shocked gas (note that the radiative cooling rate approximately rises with the square of the pre-shock density of the gas). This interaction led to a cold, highly collimated outflow accelerated up to velocities very close to the shock velocity. This material would be still now flowing and would correspond to the observed bipolar molecular outflow which, in fact, is characterized by a low temperature (~ 10 K), a large length/width ratio ($\sim$ 10–20), and a high axial velocity (paper III, Sánchez Contreras et al. 1997). The shock continued propagating to outer shells of the envelope, more and more diluted,

up to regions with very low density in which radiative cooling became inefficient. Then the hot, high pressure material started its refrigeration by an adiabatic expansion, leading to inflated shells that would be the broad emission lobes of OH 231.8+4.2. The expansion velocities superimposed to the general axial velocity gradient observed in the lobes (Sect. 4) and the relatively high temperature of these ones (inferred from the optical spectrum of the nebula, Sect. 5) are in agreement with this scenario. Moreover, the general axial velocity gradient of the emission nebula ($\sim 22\times10^{-17}$ km s^{-1} cm^{-1}) is less than that observed in the molecular outflow ($\sim 35\times10^{-17}$ km s^{-1} cm^{-1}, paper III). These figures are compatible with their respective adiabatic and radiative natures since in the adiabatic case the velocity of the shocked gas is somewhat smaller than that of the shock (e.g. Dyson & Williams 1980).

We have applied to our source the Blondin et al. (1990) criteria that allow to distinguish between radiative and adiabatic shocks. These authors define a cooling parameter, χ_s, for a shock between a jet and the ambient medium, which is the ratio of the cooling length and the jet radius. Values of $\chi_s < 1$ are theoretically indicative of radiative shocks, while $\chi_s > 1$ are obtained for adiabatic shocks. We have calculated χ_s for the south lobe of OH 231.8+4.2, assuming a jet radius of 10^{16} cm and a shock velocity of ~ 300 km s^{-1}, obtained from the molecular observations (paper III). We have also supposed that these values have not drastically changed throughout the evolution of OH 231.8+4.2. It is not possible to say the same about the pre-shock density of the gas. In fact, the density of the inner AGB circumstellar envelope on which the jet-like ejections impacted approximately 1000 yr ago, has been estimated to be $\gtrsim 10^7$ cm^{-3} (from data by Sánchez Contreras et al. 1997 and paper III). However, the density of the gas in front of the shock that accelerated the optical nebula is expected to be of the order of 10 cm^{-3} (deduced from the density of the shocked gas, Sect. 5). The two previous density values yield, respectively, $\chi_s \lesssim 10^{-5}$ and $\chi_s \sim 30$, which indicates that a transition from a radiative shock into adiabatic had to occur due to the fall of the density of the pre-shocked gas. However, it is very difficult to accurately determine when and under which conditions such a shock regime transition occurred.

We think that the bubble-like expanding structure inner to the south lobe, which is responsible for the spectral feature E (Sect. 4), was also originated by the passage of the adiabatic shock. In this context, we are probably observing the gas accelerated and excited by the passage of the forward shock (the bow-shock) and by its backward countershock. Both kind of shocks (forward and backward) have been observed in HH interstellar outflows with similar structures than those observed in OH 231.8+4.2 (e.g. Heathcote et al. 1996). The separation in two different regions, accelerated by the forward and backward shock, is supported by the different [N II]/Hα line intensity ratio found in the north and south hemispheres of the bubble-like structure (Sect. 5.1). In fact, this line ratio is larger by a factor 6 in the south hemisphere of the expanding shell, suggesting that the highest (lowest) excitation correspond to the forward (backward) shock propagating through the circumstellar medium.

We have estimated the dynamical ages of the different components of the optical nebula, the extended lobes and the bubble-like structure, considering their spatial dimensions and the expansion motion which is superimposed to the general velocity gradient (Sect. 5). Dynamical ages of ~ 500 yr have been found in both cases. This value indicates how long ago the shock regime transition took place, since the adiabatic expansion started at that time. Although the errors in this estimate can be high, the fact that we obtain dynamical ages for the ionized structures smaller than for the bipolar molecular flow (~ 1000 yr) agrees with the evolutionary picture described above in which the molecular outflow was accelerated before the appearance of the high-excitation nebula.

We would like to note that, although the proposed shock regime transition is able to explain, at least qualitatively, the morphology and kinematics of OH 231.8+4.2, the shaping and evolution of this source could be much more complicated. For example, it is expected that the passage of the fast, massive and collimated molecular outflow through the diffuse ambient medium originates a series of shock waves with extremely complex structures.

Finally, although our observations do not directly shed new light on the evolution of the central star(s) of OH 231.8+4.2, we will briefly comment on one of the most surprising aspects of this object: the presence of a cold AGB star in the core of an envelope in which the signs of the post-AGB evolution can be clearly noticed. (For example, the remarkable bipolarity and the conspicuous shocks observed are absolutely unexpected in envelopes around AGB stars.) A simple explanation (but maybe naive) to the peculiar evolution of OH 231.8+4.2 could be to attribute the ejection of the observed envelope to a very obscured companion (post-AGB) star. We recall that there is indirect evidence of a relatively hot star in the core of the nebula (Sect. 5.1). The coincidence of two stars in almost the same evolutionary status in a binary system is improbable, however, the uncommon present conditions in OH 231.8+4.2 could require such a scarce circumstance. It is also possible that, for any reason, in this object the bipolar ejections characterizing the post-AGB phase occured prematurely. This situation could also be induced by the presence of some type of companion (e.g. Morris 1987, Soker 1998). The presence of a debris disk around the star throughout its main-sequence lifetime has also been proposed to explain the collimation of the stellar wind (Kastner & Weintraub 1995). However, our NIR images of the object (paper III) reveal a weak, approximately spherical halo of emission surrounding the nebula center, that suggests that the mass loss was isotropic in the past. In any case, it is obvious that OH 231.8+4.2 is not following the usually accepted evolution from the AGB to the PN stage. Further discussion on the peculiar evolution of OH 231.8+4.2 can be found in paper III.

Acknowledgements. The Isaac Newton and Jacobus Kapteyn Telescopes are operated on the island of La Palma by the Isaac Newton Group in the Spanish Observatorio del Roque de los Muchachos of the Instituto de Astrofísica de Canarias. We are grateful to J. Zamorano and A. Gil de Paz for the images obtained with the JKT, and to J. Sanz-Forcada for its help in the spectroscopic data reduction

process with IRAF. We also thank J. Alcolea for critically reading this paper. C. Sánchez Contreras acknowledges the support of the Universidad Complutense de Madrid through a predoctoral fellowship. C. Sánchez Contreras is also grateful to the staff of the Instituto de Astrofísica de Andalucía for their hospitality during a part of the preparation of this paper. This work has been partially supported by the DGES, project numbers PB96-0104, PB95-0066, APC1998-0031, and the Junta de Andalucía.

References

Alcolea J., Bujarrabal V., Sánchez Contreras C., 1996, A&A 312, 560
Blondin J.M., Fryxell B.A., Königl A., 1990, ApJ 360, 370
Borkowski K.J., Blondin J.M., Harrington J.P., 1997, ApJ 482, L97
Bowers P.F., Morris M., 1984, ApJ 276, 646
Bujarrabal V., Alcolea J., Neri R., 1998a, ApJ 504, 915
Bujarrabal V., Alcolea J., Sahai R., Zamorano J., Zijlstra A.A., 1998b, A&A 331, 361
Cohen M., 1981, PASP 93, 288
Cohen M., Dopita M.A., Schwartz R.D., Tielens A.G.G.M., 1985, ApJ 297, 702
Dopita M.A., Sutherland R.S., 1995, ApJ 455, 468
Dopita M.A., Binette L., Schwartz R.D., 1982, ApJ 261, 183
Dyson J.E., Williams D.A., 1980, The physics of the interstellar medium. Manchester University Press, Chap. 6
Frank A., 1997, In: Habing H.J., Lamers H.J.G.L.M. (eds.) Planetary Nebulae. IAU Symp. 180, p. 225
Graham J.R., Herbst T.M., Matthews K., et al., 1993, ApJ 408, L105
Hartigan P., Raymond J. Hartmann L., 1987, ApJ 316, 323
Heathcote S., Morse J.A., Hartigan P. et al., 1996, AJ 112, 1141
Howarth I.D., 1983, MNRAS 203, 301
Huggins P.J., Bachiller R., Cox P., Forveille T., 1996, A&A 315, 284
Jackson J.M., Nguyen-Q-Rieu, 1988, ApJ 335, L83
Kastner J.H., Weintraub D.A., 1995, AJ 109, 1211
Kastner J.H., Weintraub D.A., Zuckerman B. et al., 1992, ApJ 398, 552
Kastner J.H., Weintraub D.A., Merril K.M., Gatley I., 1998, AJ 116, 1412
Morris M. 1987, PASP 99, 1115
Morris M., Guilloteau S., Lucas R., Omont A., 1987, ApJ 321, 888
Reipurth B., 1987, Nat Vol. 325, No. 6107, 787
Sánchez Contreras C., Bujarrabal V., Alcolea J., 1997, A&A 327, 689
Sánchez Contreras C., Bujarrabal V., Neri R., Alcolea J., 2000, A&A, submitted
Shure M., Sellgren K., Jones T.J., Klebe D., 1995, AJ 109, 721
Soker N., 1998, ApJ 496, 833
Zweigle J., Neri R., Bachiller R., Bujarrabal V., Grewing M., 1997, A&A 324, 624